

## Research Article

# Effects of $\text{Li}_2\text{O}$ on Structure and Viscosity of $\text{CaO-Al}_2\text{O}_3$ -Based Mold Fluxes

Lifeng Chen , Kun Liu , Peng Han, Bin Yang, and Lianghua Feng

School of Materials and Metallurgy, University of Science and Technology Liaoning, Anshan 114000, China

Correspondence should be addressed to Kun Liu; lk651206@163.com

Received 18 October 2020; Revised 17 December 2020; Accepted 13 January 2021; Published 30 January 2021

Academic Editor: Michele Benedetti

Copyright © 2021 Lifeng Chen et al. This is an open access article distributed under the Creative Commons Attribution License, which permits unrestricted use, distribution, and reproduction in any medium, provided the original work is properly cited.

Since  $\text{CaO-Al}_2\text{O}_3$ -based mold fluxes are one of the most important mold flux systems in metallurgical processes, it is important to explore their structure characteristics and viscosity. Molecular dynamics simulation is performed to study the effect of  $w(\text{CaO})/w(\text{Al}_2\text{O}_3)$  ratio on both the structural and viscosity properties of  $\text{CaO-Al}_2\text{O}_3$ -based mold fluxes. A systematic analysis of the structure and thermodynamics on  $\text{CaO-Al}_2\text{O}_3$ -based mold fluxes is carried out, and it is well known that the viscosity of mold fluxes is related to the structure. The results show that the formation of stable structures of Si-O in the mold fluxes was beneficial to reduce the probability of structural interconnection, degree of polymerization, and viscosity of the molten slag. In the cationic structure, the contents of Ca-O-Al and Ca-O-Si are more stable, the interconnection of the Ca-O-Al and Ca-O-Si network weakens, and the viscosity decreases. The tetrahedra  $[\text{AlO}_4]$  and  $[\text{SiO}_4]$  have similar structures, but they exhibit different thermodynamic and physical properties. Viscosity test shows that  $\text{CaO}/\text{Al}_2\text{O}_3 = 0.88-2$  continuously increased, when the cosolvent content  $\text{Li}_2\text{O} = 1\%-4\%$ ,  $\text{CaO-Al}_2\text{O}_3$ -based mold flux viscosity decreased, the degree of network structure polymerization decreased, and the complex structure depolymerized. Increasing the water content in the cosolvent is beneficial to reduce the viscosity of the crystallizer.

## 1. Introduction

High-manganese and high-aluminum steel is widely used in military applications, automotive manufacturing, and electrical components due to its excellent mechanical properties [1–5]; the high content of Mn and Al reduces electricity consumption, improves electromagnetic properties, and endows high strength and low density. During conventional casting production, traditional  $\text{CaO-SiO}_2$ -based mold fluxes can cause slab surface defects and interrupt the casting process by reacting with Mn and Al, decreasing  $\text{SiO}_2$  content and increasing  $\text{Al}_2\text{O}_3$  content. As a result, the physical and chemical properties of traditional  $\text{CaO-SiO}_2$ -based mold fluxes are severely deteriorated. Alternatively, low-reactivity  $\text{CaO-Al}_2\text{O}_3$ -based mold fluxes have been proposed to replace the traditional  $\text{CaO-SiO}_2$ -based mold fluxes [6–10]. In this paper, the structure of  $\text{CaO-Al}_2\text{O}_3$ -based mold fluxes is studied from the perspective of molecular dynamics.

The thermodynamic properties of  $\text{CaO-Al}_2\text{O}_3$ -based mold fluxes have been widely studied. For instance, Shi et al. showed that the viscosity increased slightly with the  $\text{CaO}/\text{Al}_2\text{O}_3$  ratio from 2 to 3, and this increase became significant with further increasing  $\text{CaO}/\text{Al}_2\text{O}_3$  ratio to 4 [11]. However, the physicochemical properties of mold fluxes have been studied from the viewpoint of thermodynamics regardless of the structure of the mold fluxes. For instance, Wang et al. have studied the influence of  $\text{B}_2\text{O}_3$  addition on the physicochemical properties of  $\text{CaO}/\text{Al}_2\text{O}_3$  mold fluxes, but the structure of mold fluxes has not been taken into account [12]. Zhang et al. have studied the effect of different molten mold fluxes on the viscosity of  $\text{CaO-Al}_2\text{O}_3$ -based mold fluxes at  $1400^\circ\text{C}$  [13]. However, the relationship between physicochemical properties and structure of the mold fluxes has not been explored. Similarly, Wang et al. have studied the influence of  $\text{CaO}/\text{Al}_2\text{O}_3$  ratio on melting temperature and viscosity of low-reactivity  $\text{CaO-Al}_2\text{O}_3$ -based mold fluxes [14]. Zhou et al. have studied the viscosity variation of  $\text{CaO-Al}_2\text{O}_3$ -based molten mold flux in the temperature of

900°C to 1300°C [15]. Shiro et al. have studied the influence of CaO and Al<sub>2</sub>O<sub>3</sub> content on the viscosity of CaO-Al<sub>2</sub>O<sub>3</sub>-based mold fluxes in the temperature range of 1550°C to 1650°C [16], but the structure of molding fluxes has not been considered. Some researchers pay attention to the effects of viscosity and structure [17–20]; it should be noted that the macroscopic properties of the continuous casting mold fluxes depend on the structure. Therefore, the effect of the CaO/Al<sub>2</sub>O<sub>3</sub> ratio in a broad range on the viscosity and structure of CaO-Al<sub>2</sub>O<sub>3</sub>-based mold fluxes must be widely studied systematically.

Therefore, the current work investigates the structure of CaO-Al<sub>2</sub>O<sub>3</sub>-B<sub>2</sub>O<sub>3</sub>-Na<sub>2</sub>O-BaO-SiO<sub>2</sub>-Li<sub>2</sub>O mold flux from the viewpoint of the molecular dynamics. Moreover, density functional theory (DFT) calculations are employed to analyze the structure and thermodynamic properties from the viewpoint of quantum mechanics and calculate the bond lengths of Li-O, Al-O, Ca-O, and Si-O. Furthermore, the thermodynamic behavior of [AlO<sub>4</sub>] and [SiO<sub>4</sub>] structures is

also studied to obtain Gibbs free energy. Moreover, in order to measure the viscosity of mold fluxes, these results theoretically provide novel insights into the structure and viscosity of mold fluxes. The aim of this study is to investigate the effect of CaO/Al<sub>2</sub>O<sub>3</sub> ratio on the CaO-Al<sub>2</sub>O<sub>3</sub>-B<sub>2</sub>O<sub>3</sub>-Na<sub>2</sub>O-BaO-SiO<sub>2</sub>-Li<sub>2</sub>O mold flux structure and viscosity and to provide further fundamental understanding of the effect of this parameter on flux properties which will be used for developing CaO-Al<sub>2</sub>O<sub>3</sub>-B<sub>2</sub>O<sub>3</sub>-Na<sub>2</sub>O-BaO-SiO<sub>2</sub>-Li<sub>2</sub>O mold flux.

## 2. Molecular Dynamics Computation

*2.1. Model Establishment of Basic Theory.* The vibrational analysis evaluation can be used to compute temperature-dependent enthalpy (H), entropy (S), vibrational free energy (G<sub>v</sub>), and constant-pressure heat capacity (C<sub>p</sub>). The heat capacity (C<sub>p</sub>) can be given as [21]

$$C_p = C_{\text{trans}} + C_{\text{rot}} + C_{\text{vib}} = R \sum_i \frac{(hv_i/kT)^2 \exp(-hv_i/kT)}{[1 - \exp(-hv_i/kT)]^2 + 4R}, \quad (1)$$

where  $C_{\text{trans}}$  refers to the translational heat capacity,  $C_{\text{rot}}$  represents the rotational heat capacity,  $C_{\text{vib}}$  denotes the vibrational heat capacity,  $R$  represents gas constant (8.314 J/mol·K),  $K$  corresponds to the Boltzmann constant,  $h$  denotes

Planck's constant,  $T$  represents the absolute temperature, and  $H$  refers to enthalpy [22]. The enthalpy ( $H$ ) can be given as

$$H = H_{\text{vib}} + H_{\text{rot}} + H_{\text{trans}} + RT = \frac{R}{2k} \sum_i hv_i + \frac{R}{K} \sum_i \frac{hv_i \exp(-hv_i/kT)}{[1 - \exp(-hv_i/kT)] + 4RT}, \quad (2)$$

where  $H_{\text{trans}}$  refers to the translational enthalpy,  $H_{\text{rot}}$  represents the rotational enthalpy, and  $H_{\text{vib}}$  denotes the vibrational enthalpy. The entropy ( $S$ ) can be given as

$$S = S_{\text{trans}} + S_{\text{rot}} + S_{\text{vib}} = \frac{5}{2} R \ln T + \frac{5}{2} R \ln w R \ln p 2.3482 + \frac{R}{2} \ln \left[ \frac{\pi}{\sqrt{\sigma}} \frac{8\pi^2 c I_A}{h} \frac{8\pi^2 c I_B}{h} \frac{8\pi^2 I_C}{h} \left( \frac{kT}{hc} \right)^3 \right] + \frac{3}{2} R + R \sum_i \frac{hv_i/kT \exp(hv_i/kT)}{1 - \exp(hv_i/kT)} - R \sum_i \ln \exp(hv_i/kT), \quad (3)$$

where  $S_{\text{trans}}$  refers to translational entropy,  $S_{\text{rot}}$  represents the rotational entropy,  $S_{\text{vib}}$  denotes the vibrational entropy,  $p$  denotes pressure,  $\sigma$  indicates symmetry number,  $c$  refers to molar concentration, and  $I_A$ ,  $I_B$ , and  $I_C$  represent the moments of inertia.  $G_v$  can be given as

$$G_v = H - T \cdot S, \quad (4)$$

$$G = G_v + E(0k),$$

$$\Delta G = G_{\text{product}} - G_{\text{reaction}}$$

where  $G_v$  refers to the vibrational free energy,  $E(0k)$  represents the total energy,  $G_{\text{product}}$  refers to the vibrational free energy product, and  $G_{\text{reaction}}$  corresponds to the vibrational free energy of the reaction.

**2.2. Calculation Method.** Based on the application of density general letter theory in quantum modernity, this paper establishes the structural calculation model and calculates the physical and chemical properties of the basic skeleton structure and complex structure. At the same time, it calculates the binding energy, total energy, and  $\Delta G$  of the structure; the structural calculation model calculates the most stable basic structure and complex structure through structural optimization, so the steps establish a calculation model as follows:

- (1) For stable basic structures and stable complex structures, it is necessary to perform vibration frequency calculations and perform geometric optimization based on statistical thermodynamics to obtain microstructures. DFT (density functional theory) calculations were utilized to compute the structure of the mold fluxes and analyze the thermodynamic properties. Finally, based on optimizing the working vibration frequency of the structure, the structure was obtained by statistical thermodynamic method.
- (2) The structural calculation model is based on quantum mechanics as the basic theory. Based on the BPW91 system in density functional theory, the basic structure and complex structure are optimized. The model uses DMol<sup>3</sup>, combines LST (linear synchronous transit)/QST (quadratic synchronous transit) with CGM (conjugate gradient methods), and then adopts the transition method. The most stable structure was searched for.
- (3) The optimization calculation of the structural calculation model is based on DFT's DMol<sup>3</sup> quantum mechanics module, which can accurately obtain the parameters of molecular structure and physical and chemical properties. The stabilized structures were used, as reactants, to explore the transition states via complete LST (linear synchronous transit) and QST (quadratic synchronous transit) methods. The SCF (self-consistent field) method was used with a total energy.

### 3. Structure Properties

**3.1. Analysis of Structures and Thermodynamic Properties.** The structure should be studied because the physicochemical properties of CaO-Al<sub>2</sub>O<sub>3</sub>-SiO<sub>2</sub> slag are inseparable from the structure [13, 23–26]. Here, Si-O and Al-O exist as an aluminosilicate structure. The bond length and bond energy of Al-O, Ca-O, Si-O, and Li-O are summarized in Table 1. In addition, the bond length in the Al-O unit (1.65 Å) is larger than that in the Si-O unit (1.53 Å), the bond length in the Li-O unit (2.05 Å) is larger than that in the Si-O unit (1.53 Å),

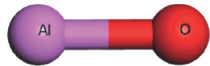
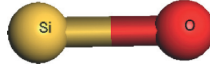
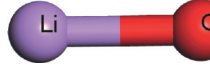
and the bond energy of Si-O bond (−853.48 kJ/mol) is lower than that of Al-O and Li-O. The lower the binding energy and total energy, the more stable the structure. Therefore, Si-O is more stable than Al-O and Li-O, the basic framework structure of mold flux cosolvent SiO<sub>2</sub> is Si-O, and adding the Si-O structure to the slag structure is beneficial to the stability of the physical and chemical properties of the mold slag, thus reducing the possibility of the simple structure in the slag being transformed into a complex structure.

Figure 1 shows the change in  $\Delta G$  of anionic structure and cationic structure with respect to temperature; the structures become less stable with higher temperatures. The reaction that produces a O-Si-O structure has the greatest  $\Delta G$  trend, while the reaction that produces Si-O-Si structures has lesser  $\Delta G$  tendency; therefore, it is easier to generate O-Si-O structure in the mold fluxes.

The thermodynamic behavior of the structure mainly determines the structure of mold fluxes. Figure 2 shows the total energy of the anionic structure and cationic structure. Herein, the results indicate structure diversity and different physical characteristics. The results indicate that O-Al-O is more stable than Al-O-Al. Ca-O-Si structure is stable, it is difficult to form complex structure, and the polymerization of slag is reduced, resulting in weak connection of the molten fluxes. The viscosity of the mold flux decreases with CaO content increasing, because the free O<sup>2-</sup> ions released by O<sup>2-</sup> ions can enter cosolvent Al<sub>2</sub>O<sub>3</sub> bond and form the O-Al-O structure, which causes the relatively reduced connections of the structure of the mold flux and the reduction in mold flux viscosity. Figure 3 shows the change in  $\Delta G$  of different structures with respect to temperature; it can be readily observed that the  $\Delta G$  increases with increasing temperature, the structures become less stable with higher temperatures, and the increasing temperature reformed the flux network through the breakages of structure consisting complex structure linkages, as well as the reduction in molten slag viscosity. If the structure consisting of complex increases and hinders the depolymerization of the structure, the viscosity of mold fluxes is increased due to complex structure.

**3.2. Analysis of Tetrahedral Structure and Thermodynamic Properties.** It should be noted that [AlO<sub>4</sub>] and [SiO<sub>4</sub>] are the basic tetrahedron structure units of the CaO-Al<sub>2</sub>O<sub>3</sub>-based mold fluxes. In the aluminate melt structure, Al<sub>2</sub>O<sub>3</sub> exhibits a tetrahedral structure and octahedral structure, as Al<sub>2</sub>O<sub>3</sub> has amphoteric characteristics in mold flux. It exists as a [AlO<sub>4</sub>] network structure in alkaline melt. Moreover, the addition of SiO<sub>2</sub> promotes the incorporation of Si into Al<sub>2</sub>O<sub>3</sub> structure. The reason is that the pickup of Al<sub>2</sub>O<sub>3</sub> will increase Al-O complex structure and form the bond of Al-O-Si to raise the polymerization degree of the molten slag, which results in greater viscosity flow resistance and increased viscosity. In terms of molten flux, CaO decomposes to form Ca ions and free oxygen, where the former compensates for charge difference between [AlO<sub>4</sub>] and [SiO<sub>4</sub>], and the later forms a depolymerization structure with nonbridging oxygen; the viscosity is decreased due to the low polymerization.

TABLE 1: The structure and energy of Al-O, Li-O, and Si-O.

Structure	Bond energy (kJ/mol)	Total energy (kJ/mol)	Bond length (Å)	Chart
Al-O	-576.5	-833915.87	1.65	
Si-O	-853.48	-957628.72	1.53	
Li-O	-329.6	-217003.5	2.05	

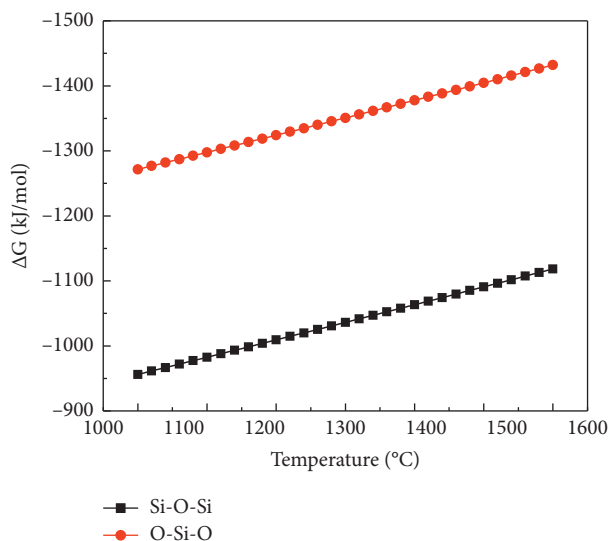
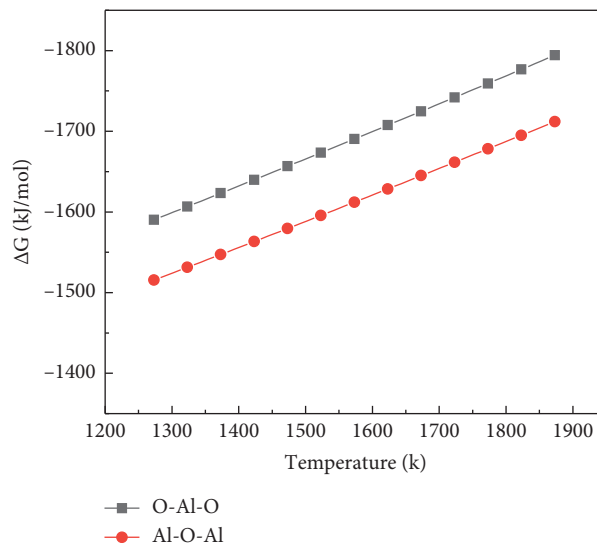
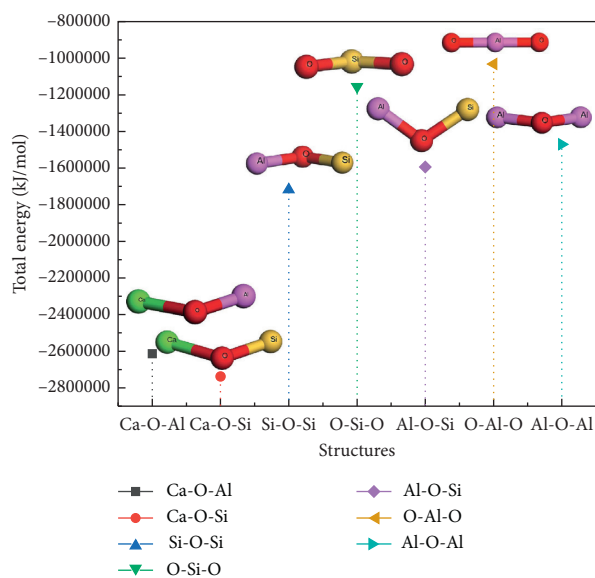
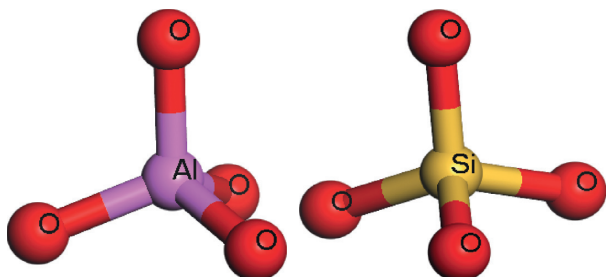
FIGURE 1: The change in  $\Delta G$  of Si-O-Si and O-Si-O structures with respect to temperature.FIGURE 3: The change in  $\Delta G$  of different structures with respect to temperature.

FIGURE 2: Structural diagram showing total energy of Ca-O-Al, Ca-O-Si, Si-O-Si, O-Si-O, Al-O-Si, O-Al-O, and Al-O-Al.

As is shown in Table 2, in addition, the bond length in the  $[\text{AlO}_4]$  tetrahedral unit is larger than that in the  $[\text{SiO}_4]$  tetrahedral unit; however, the total energy and bond energy of  $[\text{SiO}_4]$  tetrahedral are smaller than  $[\text{AlO}_4]$ , and the bond angle of  $[\text{AlO}_4]$  and  $[\text{SiO}_4]$  structures is  $109.47^\circ$ . The results indicate that Si-O is more stable than Al-O; despite the fact that both  $[\text{AlO}_4]$  and  $[\text{SiO}_4]$  exhibit the same tetrahedral structure and basic network, the stability of  $[\text{AlO}_4]$  tetrahedral network is not as good as  $[\text{SiO}_4]$ , and the possibility of  $[\text{SiO}_4]$  structure transition to complex structure is reduced. This indicate that  $[\text{SiO}_4]$  is more stable than  $[\text{AlO}_4]$ ; hence, the  $[\text{SiO}_4]$  difficulty forming complex structures, which causes the weaker link of the molten fluxes. As shown in Figure 4, although the structures of the  $[\text{AlO}_4]$  and  $[\text{SiO}_4]$  are similar,  $[\text{AlO}_4]$  requires more thermal energy to depolymerize than  $[\text{SiO}_4]$ , both  $[\text{AlO}_4]$  and  $[\text{SiO}_4]$  exhibited different thermodynamic and physical properties, and  $[\text{SiO}_4]$  is more stable than  $[\text{AlO}_4]$ . The effect of aluminosilicate structures becomes important because of high  $\text{Al}_2\text{O}_3$  content; in the aluminosilicate structure, the  $[\text{AlO}_4]$  tetrahedron structures increased, the stability of the structures is reduced, and the viscosity is increased due to the high polymerization.

TABLE 2: The structure and energy of  $[\text{AlO}_4]$  and  $[\text{SiO}_4]$ .

Structure	Total energy (kJ/mol)	Bond length (Å)	Bond energy (kJ/mol)	Bond angle
$[\text{AlO}_4]$	-1425883.16	1.76	-1378.35	109.47°
$[\text{SiO}_4]$	-1549766.36	1.63	-1825.73	109.47°

FIGURE 4: Structures of  $[\text{AlO}_4]$  and  $[\text{SiO}_4]$ .

Hence, the viscosity is increased due to the high polymerization and hindered ionic mobility.

## 4. Experimental

**4.1. Sample Preparation and Viscosity Measurement.** Table 3 shows the chemical composition of the  $\text{CaO-Al}_2\text{O}_3$ -based mold fluxes before heating; reagent grade powders of  $\text{CaO}$ ,  $\text{Al}_2\text{O}_3$ ,  $\text{B}_2\text{O}_3$ ,  $\text{Na}_2\text{O}$ ,  $\text{BaO}$ ,  $\text{SiO}_2$ , and  $\text{Li}_2\text{O}$  were used as raw materials, and chemical reagents are pure reagents (>95.5%).  $\text{CaO}$  was calcined at  $800^\circ\text{C}$  in a muffle furnace for 8 h, and other powders were placed at  $500^\circ\text{C}$ . Then 1wt%, 2wt%, 3wt%, and 4wt%  $\text{Li}_2\text{O}$  were added to the  $\text{CaO-Al}_2\text{O}_3$ -based mold fluxes, and four experimental samples were obtained.

The viscous behavior of the  $\text{CaO-Al}_2\text{O}_3$ -based mold fluxes with various concentrations of  $\text{Li}_2\text{O}$  has been studied using the viscosity measurement method to understand the effects on the viscosity with these additives, and the viscosity of mold fluxes was measured by using a rotating cylindrical viscometer. The schematic diagram is shown in Figure 5. The Mo spindle was rotating at a fixed speed of 15r/min, a Pt/Rh thermocouple was placed right beneath the bottom of a high-purity graphite crucible, 150g flux sample was placed in the crucible and heated to  $1350^\circ\text{C}$ , it decreased with a rate of  $5^\circ\text{C}/\text{min}$ , and the viscosity of experimental flux was continuously recorded.

**4.2. Effect of  $\text{CaO}/\text{Al}_2\text{O}_3$  Ratio on Flux Viscosity.** Figure 6 shows a diagram of network changes. As the  $\text{CaO}$  content increases, the viscosity of the mold flux decreases, which is because the free  $\text{Ca}^{2+}$  released by  $\text{CaO}$  can break O-Al-O and Al-O-Al bond and form stable structure the Ca-O-Al and Ca-Al-O structure, which results in a relatively reduced connection of the structure and a decrease in the viscosity of the mold fluxes. The  $\text{CaO}$  and  $\text{Al}_2\text{O}_3$  content is very important to control the viscosity of mold flux, while this effect would be attenuated with the excessive addition of  $\text{CaO}$  and  $\text{Al}_2\text{O}_3$ , although the viscosity can be

TABLE 3: The chemical composition of the  $\text{CaO-Al}_2\text{O}_3$ -based mold fluxes.

Sample no.	$\text{CaO}/\text{Al}_2\text{O}_3$	Chemical composition (wt%)				
		$\text{B}_2\text{O}_3$	$\text{Na}_2\text{O}$	$\text{BaO}$	$\text{SiO}_2$	$\text{Li}_2\text{O}$
A1	0.88	10	9	10	6	1
A2	1.25	10	9	10	6	2
A3	1.61	10	11	10	6	3
A4	2	10	10	10	6	4

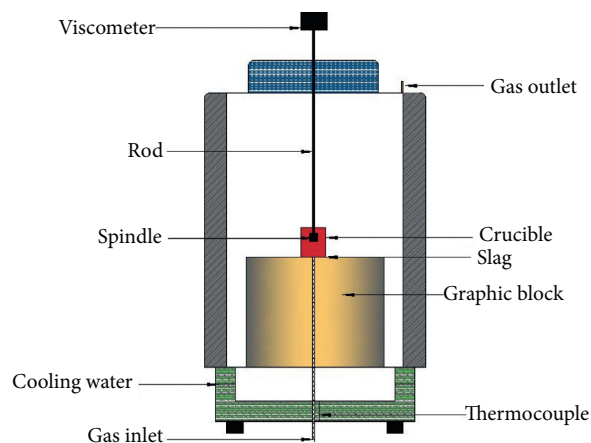
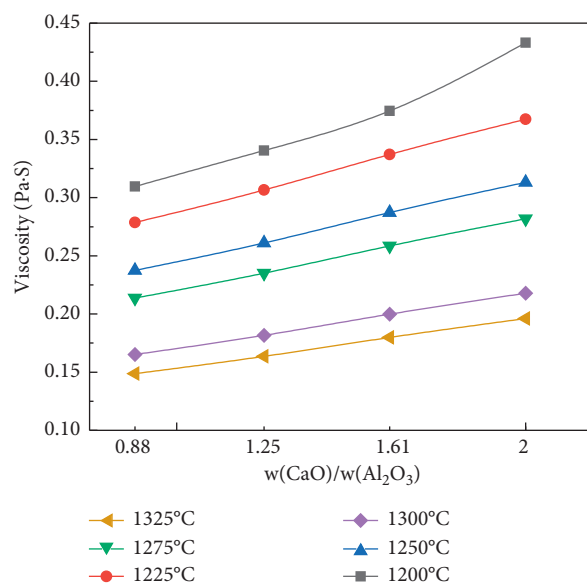


FIGURE 5: Schematic of experimental setup.

FIGURE 6: Viscosity of mold fluxes versus  $\text{CaO}/\text{Al}_2\text{O}_3$  ratio at different temperatures.

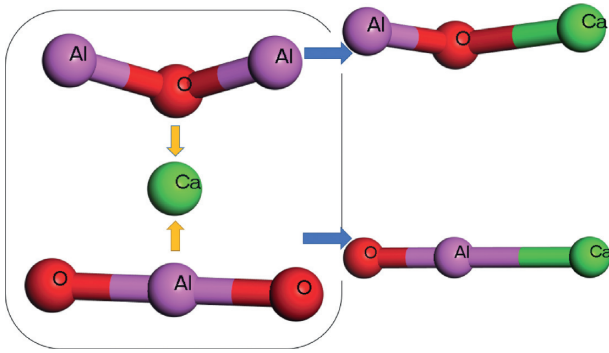


FIGURE 7: Schematic diagram for the changes of the network.

increased by adding excessive addition of  $\text{Al}_2\text{O}_3$ . Figure 7 shows the viscosity of mold fluxes versus  $w(\text{CaO})/w(\text{Al}_2\text{O}_3)$  in the temperature range from  $1200^\circ\text{C}$  to  $1325^\circ\text{C}$  and the effect of  $\text{CaO}/\text{Al}_2\text{O}_3$  ratio on the viscosity of sample A1 to A4. The results show that the viscosity of the slags decreased with the increase in  $\text{CaO}/\text{Al}_2\text{O}_3$  ratio. It can be seen from Figure 7 that the viscosity of the melt decreased with increasing  $\text{CaO}/\text{Al}_2\text{O}_3$  ratio from 0.88 to 2. The continuous addition of  $\text{CaO}$  into the aluminates instigated the weakening of the structures of  $[\text{AlO}_4]$ , and it should be noted that the content of  $\text{Ca}^{+}$  ions in the mold fluxes is enough for charge compensation. When  $\text{CaO}$  content increases, the content of  $\text{Ca}^{+}$  ions increased and destroyed the structure.

Figure 8 shows the effect of sample on the viscosity of the mold fluxes; the temperature rise reduced the viscosity of the mold fluxes, which reduces the viscosity and facilitates structure depolymerization. Figure 9 shows the viscosity of samples A1 to A4 in the mold fluxes with various  $\text{Li}_2\text{O}$  contents. Meanwhile,  $\text{Li}_2\text{O}$  could also stabilize the structural unit of  $\text{Li-O}$  structures by link aluminate.  $\text{Li}_2\text{O}$  could release  $\text{O}^{2-}$  ions to break the complex structure into simple structure. The schematic diagram for the changes of the  $[\text{AlO}_6]$  is shown in Figure 10; the stability of  $[\text{AlO}_4]$  tetrahedral network is not as good as  $[\text{AlO}_6]$ , and the possibility of  $[\text{AlO}_6]$  structure transition to complex structure is reduced. Moreover, increasing  $\text{CaO}/\text{Al}_2\text{O}_3 = 0.88-2$  leads to an increase in the fraction of  $[\text{AlO}_6]$  octahedron but a decrease in the fraction of  $[\text{AlO}_4]$  tetrahedron, and the higher content of  $\text{CaO}$  destroys the structure of  $[\text{AlO}_4]$  and, consequently, reduces the viscosity. The changes of the  $[\text{SiO}_4]$  are shown in the schematic diagram in Figure 11; the  $\text{O}^{2-}$  from  $\text{CaO}$  reacts with the electropositive  $\text{Si}$  ion from  $\text{SiO}_2$  and generates stable structure  $[\text{SiO}_4]$ , the complex structure transforms into a simple structure, the stability of  $[\text{AlO}_4]$  tetrahedral network is not as good as  $[\text{SiO}_4]$ , the possibility of  $[\text{SiO}_4]$  structure transition to complex structure is reduced, the alkaline oxide determines the structural properties of the mold fluxes, which are also influenced by the structure, and the structure of  $[\text{AlO}_4]$  high melting substances leads to the formation of the complex structure, increase the degree of polymerization, and increases the viscosity of the mold fluxes. It should be noted that the viscosity of the mold fluxes is also affected by the polymerization, and the microstructure of the high polymerization can lead to a high

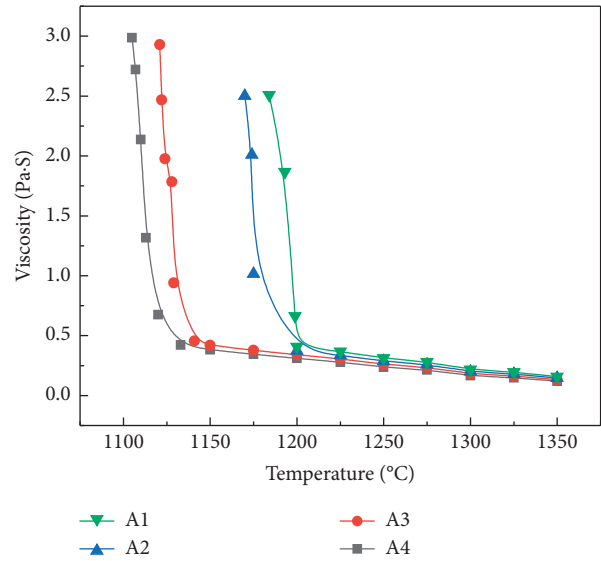


FIGURE 8: Viscosity of mold fluxes as a function of  $\text{Li}_2\text{O}$  content under various temperature conditions.

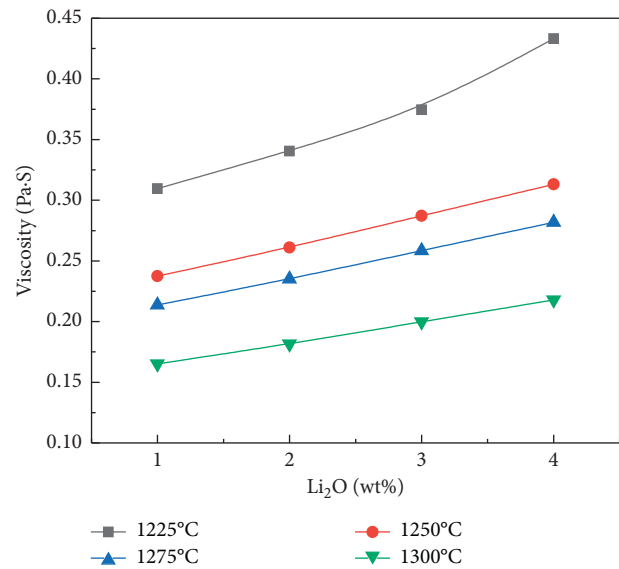


FIGURE 9: Viscosity of samples A1 to A4 in the fully fluid region with various  $\text{Li}_2\text{O}$  contents.

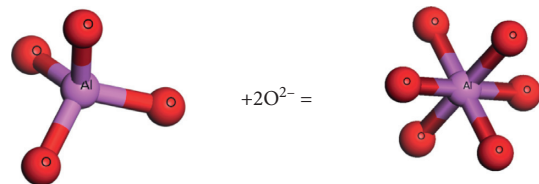


FIGURE 10: Schematic diagram for the changes of the  $[\text{AlO}_6]$ .

viscosity, if it can be structurally depolymerized, resulting in a decrease in viscosity.

As can be seen, as the  $\text{CaO}/\text{Al}_2\text{O}_3$  content decreases, the viscosity of the slag gradually increases, and as the  $\text{Li}_2\text{O}$  content decreases, the viscosity of the slag increases. Within

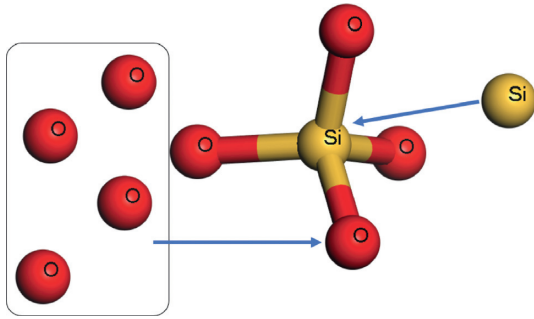


FIGURE 11: Schematic diagram for the changes of the  $[\text{SiO}_4]$ .

the experimental temperature range of  $1225^\circ\text{C}$  to  $1300^\circ\text{C}$ , the viscosity of the slag decreased with addition of  $\text{Li}_2\text{O}$ . The  $\text{Li}_2\text{O} = 1-2$  significantly lowered the viscosity, and further addition of  $\text{Li}_2\text{O} = 2-4$  significantly lowered the viscosity. The change in  $\text{Li}_2\text{O}$  concentration releases Li ions from the mold fluxes, the complex structure is transformed into a simple structure, and the viscosity of mold fluxes is influenced by the complex anions. Therefore, the viscosity of the mold fluxes can be controlled by adjusting the polymerization of the structure. It should be noted that the dissociation of simple structures increases the fluidity of the melt, as excessive  $\text{O}^{2-}$  does not have a significant effect on the less polymerized network structure but rather leads to an increase in viscosity.

**4.3. Viscous Flow Activation Energy.** The mold flux temperature is higher than the break temperature, which can be considered as a Newtonian fluid, so the viscosity changes with temperature follow the Arrhenius equation:

$$\eta = A \exp\left(\frac{E_a}{RT}\right), \quad (5)$$

$$\ln \eta = \frac{E_a}{RT} + \ln A, \quad (6)$$

where  $T$  is temperature,  $\text{K}$ ;  $A$  is constant;  $E_a$  is activation energy,  $\text{kJ/mol}$ ; and  $R$  is perfect gas constant,  $8.314 \text{ J/mol}\cdot\text{K}$ .

The optical basicity ( $\Lambda$ ) can characterize the ‘usability’ of providing  $\text{O}^{2-}$ , which explains the degree of polymerization of the mold fluxes. The corrected optical basicity ( $\Lambda_{\text{corr}}$ ) was proposed by Mills to charge balance the  $\text{Al}^{3+}$  ions or the  $\text{Si}^{4+}$  chain or ring [28]. In the calculation shown in formula (7), corrected optical basicity proposed by Mills ( $\Lambda_{\text{corr}}$ ),  $\Lambda$  is the optical basicity;  $X$  is the mole fraction;  $n$  is the number of slag oxygen atoms in component molecule; and  $\Lambda_{\text{corr}}$  is the corrected optical basicity.

$$\lambda_{\text{corr}} = \frac{\sum(X_1 n_1 \lambda + X_2 n_2 \lambda + X_3 n_3 \lambda + X_4 n_4 \lambda \dots)}{\sum(X_1 n_1 + X_2 n_2 + X_3 n_3 + X_4 n_4 \dots)}. \quad (7)$$

Formula (6) shows the linear relationship between  $\ln \eta$  and  $1/T$  in the Newtonian fluid region, to obtain activation energy. Table 4 shows change trend of melting temperature and break temperature of slags A1, A2, A3, and A4 corresponding to the change trend of activation energy. In addition, the molten slag is in a completely liquid state and is a Newtonian fluid, and the activation energy can be estimated using the Arrhenius

TABLE 4: Melting temperature ( $T_m$ ), break temperature ( $T_b$ ), corrected optical basicity ( $\Lambda_{\text{corr}}$ ), and viscous activation energy of experimental slags.

Sample no.	$T_m$ ( $^\circ\text{C}$ )	$T_b$ ( $^\circ\text{C}$ )	$\Lambda_{\text{corr}}$	$E_a$ ( $\text{kJ/mol}$ )
A1	1133	1202	0.65	142
A2	1121	1183	0.69	123
A3	1084	1132	0.72	112
A4	1088	1121	0.74	92

equation. Break temperature is closely related to activation energy and bond breakage of composite negative ions in mold fluxes at elevated temperature; the polymerization degree decreases and the migration energy increases. The viscosity of the mold fluxes is usually reduced as the corrected optical alkalinity increases. This is higher than those by Li al [27]. In the experimental research of mold fluxes, the different network structures of the mold fluxes of other researchers and authors lead to different activation energy.

## 5. Conclusions

This work investigated the variations of structure, thermodynamic properties, and viscosity of  $\text{CaO-Al}_2\text{O}_3$ -based mold fluxes. The following conclusions can be drawn:

- (1) The Si-O is more stable than Li-O, and Al-O is not easily linked to other structures, relatively weakening the mold flux structure and lowering the degree of polymerization. The B-O is more stable than Al-O, which is not easily linked to other structures, relatively weakening the mold flux structure and lowering the degree of polymerization, resulting in relatively reduced connections of the structure of the mold flux and the reduction in mold flux viscosity. While this effect would be attenuated with the excessive addition of  $\text{Al}_2\text{O}_3$ , the complex structure is more likely to exist in the  $\text{CaO-Al}_2\text{O}_3$ -based mold fluxes.
- (2) The viscous behavior of the  $\text{CaO-Al}_2\text{O}_3$ -based mold flux system with various concentrations of  $\text{Li}_2\text{O}$  has been studied using the viscosity measurement method. The increased  $\text{Li}_2\text{O}$  in the mold fluxes destroys the network structure and reduces the polymerization degree and the transition from complex structure to simple structure. The viscosity of the mold fluxes usually decreases with the increase of corrected optical basicity. This report shows the importance of exploring and establishing the relationship between the performance and structure of the mold fluxes from a structural perspective.

## Data Availability

The data (figures) that support the findings of this study are available upon request from the corresponding author.

## Conflicts of Interest

The authors declare that there are no conflicts of interest regarding the publication of this paper.

## Acknowledgments

The authors are grateful for the financial support by the National Key R&D Project of China (no. 2017YFC0805100) and Science and Technology Projects of Liaoning Province (no. 2018307003). The project was supported by the State Key Laboratory of Metallic Materials for Offshore Equipment and Applications (no. 2017-01-04).

## References

- [1] Y. Li, Z. Lin, A. Jiang, and G. Chen, "Use of high strength steel sheet for lightweight and crashworthy car body," *Materials and Design*, vol. 24, no. 3, pp. 177–182, 2003.
- [2] K. Zhang, J. Liu, and H. Cui, "Investigation on the slag-steel reaction of mold fluxes used for casting Al-TRIP steel," *Metals*, vol. 9, pp. 398–412, 2003.
- [3] G. Frommeyer, U. Brück, and P. Neumann, "Supra-ductile and high-strength manganese-trip/twip steels for high energy absorption purposes," *ISIJ International*, vol. 43, no. 3, pp. 438–446, 2003.
- [4] X. J. Chen, C. Yang, and Z. Zhi, "Continuous casting of high-Al steel in shougang jingtang steel works," *Metals*, vol. 22, pp. 53–56, 2015.
- [5] X. Yu, G.H. Wen, P. Tang, F.J. Ma, and H. Wang, "Behavior of mold slag used for 20Mn23Al nonmagnetic steel during casting," *Journal of Iron and Steel Research International*, vol. 18, no. 1, pp. 20–25, 2011.
- [6] J. Liu, M. Guo, P. Jones, F. Verhaeghe, B. Blanpain, and P. Wollants, "in situ observation of the direct and indirect dissolution of MgO particles in CaO-Al<sub>2</sub>O<sub>3</sub>-SiO<sub>2</sub>-based slags," *Journal of The European Ceramic Society*, vol. 27, p. 1972, 2007.
- [7] Z. Li, G. Ma, M. Liu, and J. Zou, "Calculation model for activity of FeO in quaternary slag system SiO<sub>2</sub>-CaO-Al<sub>2</sub>O<sub>3</sub>-FeO," *Metals*, vol. 8, pp. 724–734, 2018.
- [8] C. Liu, X. Liu, X. Yang, H. Zhang, and M. Zhong, "Kinetics of MgO reduction in CaO-Al<sub>2</sub>O<sub>3</sub>-MgO slag by Al in liquid Fe," *Metals*, vol. 9, pp. 998–1012, 2019.
- [9] J. Yang, D. Chen, M. Long, and H. Duan, "An approach for modelling slag infiltration and heat transfer in continuous casting mold for high Mn-high Al steel," *Metals*, vol. 10, pp. 998–1012, 2020.
- [10] L. Zhirong, J. Boran, Z. Yabing, H. Shengping, W. Qiangqiang, and W. Qian, "Dissolution behaviour of Al<sub>2</sub>O<sub>3</sub> in mould fluxes with low SiO<sub>2</sub> content," *Ceramics International*, vol. 45, no. 3, pp. 4035–4042, 2019.
- [11] L. Wang, J. Cui, J. Yang, C. Zhang, and D. Cai, "Melting properties and viscosity of SiO<sub>2</sub>-CaO-Al<sub>2</sub>O<sub>3</sub>-B<sub>2</sub>O<sub>3</sub> system," *Steel Research*, vol. 86, pp. 670–677, 2014.
- [12] C.-B. Shi, M.-D. Seo, J.-W. Cho, S.-H. Kim, and H. G. Lee, "Crystallization characteristics of CaO-Al<sub>2</sub>O<sub>3</sub>-based mold flux and their effects on in-mold performance during high-aluminum TRIP steels continuous casting," *Metallurgical and Materials Transactions B*, vol. 45, no. 3, pp. 1081–1097, 2014.
- [13] L. Zhang, W.L. Wang, and H.-Q. Shao, "Review of non-reactive CaO-Al<sub>2</sub>O<sub>3</sub>-based mold fluxes for casting high-aluminum steel," *Journal of Iron and Steel Research International*, vol. 26, no. 4, pp. 336–344, 2019.
- [14] Q. Wang, J. A. Yang, C. Zhang, D. X. Cai, J. Q. Zhang, and O. Ostrovski, "Effect of CaO/Al<sub>2</sub>O<sub>3</sub> ratio on viscosity and structure of CaO-Al<sub>2</sub>O<sub>3</sub>-based fluoride-free mould fluxes," *Journal of Iron and Steel Research International*, vol. 26, pp. 374–384, 2019.
- [15] L. Zhou and W. Wang, "Application of non-arrhenius models to the viscosity of mold flux," *Metallurgical and Materials Transactions B*, vol. 47, no. 3, pp. 1548–1552, 2016.
- [16] B. Y. Shiro, H. Makoto, K. Tetsuro, I. Takeshi, and H. Mitsutaka, "Sulphide capacity and sulphur solubility in CaO-Al<sub>2</sub>O<sub>3</sub> and CaO-Al<sub>2</sub>O<sub>3</sub>-CaF<sub>2</sub> slags," *ISIJ International*, vol. 47, pp. 1548–1552, 2016.
- [17] Z. Lei, "The evolution of the mold flux melt structure during the process of fluorine replacement by B<sub>2</sub>O<sub>3</sub>," *Journal of the American Ceramic Society*, vol. 103, pp. 112–121, 2020.
- [18] M. Sajid, C. Bai, W. Yu, Z. You, M. Tan, and M. Aamir, "First principle study of electronic structural and physical properties of CaO-SiO<sub>2</sub>-Al<sub>2</sub>O<sub>3</sub> ternary slag system by using Ab Initio molecular and lattice dynamics - ScienceDirect," *Journal of Non-crystalline Solids*, vol. 550, Article ID 120384, 2020.
- [19] C. Lifeng, L. Kun, P. Han, B. Yang, and L. Feng, "Calculation and analysis of the structure and viscosity of B<sub>2</sub>O<sub>3</sub>-regulated CaO-Al<sub>2</sub>O<sub>3</sub>-based mold fluxes," *Journal of Chemistry*, vol. 2020, Article ID 8844392, 10 pages, 2020.
- [20] Y. Jian, J. Zhang, O. Ostrovski, C. Zhang, and D. Cai, "Effects of fluorine on solidification, viscosity, structure, and heat transfer of CaO-Al<sub>2</sub>O<sub>3</sub>-based mold fluxes," *Metallurgical and Materials Transactions B*, vol. 50, no. 4, pp. 1766–1772, 2019.
- [21] J. Sanchez, H. Schreyer, D. Sulsky, and P. Wallstedt, "Solving quasi-static equations with the material-point method," *International Journal for Numerical Methods in Engineering*, vol. 103, no. 1, pp. 60–78, 2015.
- [22] D. Sulsky, S.-J. Zhou, and H. L. Schreyer, "Application of a particle-in-cell method to solid mechanics," *Computer Physics Communications*, vol. 87, no. 1-2, pp. 236–252, 1995.
- [23] M. Valdez, K. Prapakorn, A. V. Cramb, and S. Seetharaman, "A study of the dissolution of Al<sub>2</sub>O<sub>3</sub>, MgO and MgAl<sub>2</sub>O<sub>4</sub> particles in a CaO-Al<sub>2</sub>O<sub>3</sub>-SiO<sub>2</sub> slag," *Steel Research*, vol. 78, no. 8, pp. 291–297, 2001.
- [24] H. S. Park, H. Kim, and I. Sohn, "Influence of CaF<sub>2</sub> and Li<sub>2</sub>O on the Viscous Behavior of Calcium Silicate Melts Containing 12 wt pct Na<sub>2</sub>O," *Metallurgical and Materials Transactions B*, vol. 42, no. 2, pp. 324–330, 2011.
- [25] J. Li, Q. Shu, X. Hou, and K. Chou, "Effect of TiO<sub>2</sub>," *ISIJ International*, vol. 55, pp. 830–836, 2015.
- [26] G. Fan, S. He, T. Wu, and Q. Wang, "Effect of fluorine on the structure of high Al<sub>2</sub>O<sub>3</sub>-bearing system by molecular dynamics simulation," *Metallurgical and Materials Transactions*, vol. 46, pp. 2005–2013, 2015.
- [27] Z. Li, X. You, M. Li, and Q. Wang, "Effect of substituting CaO with BaO and CaO/Al<sub>2</sub>O<sub>3</sub> ratio on the viscosity of CaO-BaO-Al<sub>2</sub>O<sub>3</sub>-CaF<sub>2</sub>-Li<sub>2</sub>O mold flux system," *Metals*, vol. 9, pp. 1–13, 2019.